Proceedings of the ASME 2010 3rd Joint US-European Fluids Engineering Summer Meeting and 8th International Conference on Nanochannels, Microchannels, and Minichannels
FEDSM-ICNMM2010
August 1-5, 2010, Montreal, Canada

FEDSM-ICNMM2010-30678

EFFICIENT ESTIMATION OF THE FRICTION FACTOR FOR FORCED LAMINAR FLOW IN AXIALLY SYMMETRIC CORRUGATED PIPES

Patricio I. Rosen Esquivel*
CASA†
Department of Mathematics and Computer Science
Eindhoven University of Technology
Eindhoven, The Netherlands
Email: p.i.rosenesquivel@tue.nl

Jan H.M. ten Thije Boonkkamp
CASA
Department of Mathematics and Computer Science
Eindhoven University of Technology
Eindhoven, The Netherlands
Email: tenthije@win.tue.nl

Jacques A.M. Dam
Stork FDO Inoteq
Amsterdam, The Netherlands
Email: jacques.dam@stork.com

Robert M.M. Mattheij
CASA
Department of Mathematics and Computer Science
Eindhoven University of Technology
Eindhoven, The Netherlands
Email: r.m.m.mattheij@tue.nl

ABSTRACT

In this paper we present an efficient method for calculating the friction factor for forced laminar flow in arbitrary axially symmetric pipes. The approach is based on an analytic expression for the friction factor, obtained after integrating the Navier-Stokes equations over a segment of the pipe. The friction factor is expressed in terms of surface integrals over the pipe wall, these integrals are then estimated by means of approximate velocity and pressure profiles computed via the method of slow variations. Our method for computing the friction factor is validated by comparing the results, to those obtained using CFD techniques for a set of examples featuring pipes with sinusoidal walls. The amplitude and wavelength parameters are used for describing their influence on the flow, as well as for characterizing the cases in which the method is applicable. Since the approach requires only numerical integration in one dimension, the method proves to be much faster than general CFD simulations, while predicting the friction factor with adequate accuracy.

1 INTRODUCTION

The effect of wall shape on the friction factor of forced flow through pipes and hoses is of interest in many applications such as LNG transfer hoses [1]. Several numerical and experimental studies have shown that the contribution of wall shape is not trivial, even in the laminar case. If wall shape of corrugated pipes is translated into an equivalent wall roughness, it is found that the friction factor differs considerably from the values obtained from the classical Moody diagram [2].

Despite the wide use of corrugated pipes or hoses, the effects of wall shape on the flow are commonly obtained from one-phase flow pressure drop experiments or CFD computational experiments. For optimization of flow paths however, both methods soon become non affordable and faster calculation methods are required. The study of flow in non-straight pipes dates back to Nikuradse's experiments [3], whose results obtained from artificially roughened pipes were later arranged in the more well-

*Address all correspondence to this author.
†Centre for Analysis, Scientific Computing and Applications.

known form of the Moody Diagram [2]. In the Moody diagram, the friction factor for laminar flow appears as independent of wall roughness, but in general the friction factor for laminar flow in corrugated pipes has been found to be dependent on the specific wall shape [4–6].

Several approaches for the calculation of flow in corrugated pipes have been suggested, among the ones based on CFD, we mention the publications by Mahmud et al. [7] and Blackburn et al. [6] for the case of laminar flow, and the publications by Pisarenco et al. [8] and Van der Linden et al. [9], for turbulent flow. Still, even after reducing the domain of calculation to one single period in two dimensions, the computational costs can still be high for certain situations, for instance, when one is interested in optimization of flow paths, or in performing calculations for a large network of interconnected hydraulic components.

In this paper we develop a method for estimating the Darcy friction factor in axially symmetric pipes of arbitrary shape. The method is accurate and very efficient because it only requires numerical integration in one dimension. The range of applicability of the method is discussed and presented via a comparison with a set of numerical examples. The paper is organized as follows. We start by presenting the governing equations and geometry. Directly from the governing equations, we derive an analytical expression for the friction factor in terms of surface integrals over the pipe wall. In order to compute or approximate these integrals, we require the solution for the pressure and the axial velocity component at the wall of the pipe. We solve this problem by using approximate solutions for the pressure and the velocity, obtained via the method of slow variations. For completeness we include the derivation of this asymptotic expansions. Based on this expansion we finally obtain approximate formulas for estimating the friction factor. Finally the accuracy of the method is studied and discussed.

2 GOVERNING EQUATIONS

We consider the Navier-Stokes equations for steady, incompressible, axially symmetric, laminar flow in cylindrical coordinates

$$UU_X + VU_R = \nu\left(U_{XX} + U_{RR} + \frac{1}{R}U_R\right) - \frac{1}{\rho}P_X, \tag{1a}$$

$$UV_X + VV_R = \nu\left(V_{XX} + V_{RR} + \frac{1}{R}V_R - \frac{1}{R^2}V\right) - \frac{1}{\rho}P_R, \tag{1b}$$

$$U_X + V_R + \frac{1}{R}V = 0, \tag{1c}$$

where the corresponding variables are the axial coordinate X, the radial coordinate R, the axial velocity U, the radial velocity V, and the pressure P. The constants ν and ρ represents the kinematic viscosity and the density of the fluid, respectively. The angular component does not play a role due to the assumption of axially symmetric flow.

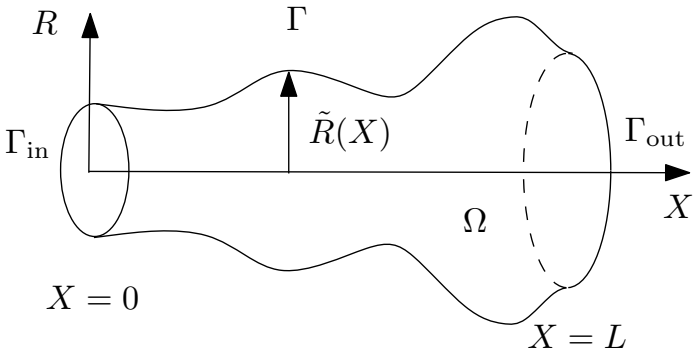

FIGURE 1. Axisymmetric pipe with center line along the X-axis. Γ stands for the wall of the pipe, Γ_{in} for the cross section at $X = 0$ and Γ_{out} the cross section at $X = L$

The geometry under consideration is an axially symmetric pipe, depicted as in Figure 1. The location of the wall of the pipe, can be described in terms of the cylindrical basis vectors $\mathbf{e}_R$, $\mathbf{e}_\Theta$, $\mathbf{e}_X$, via the parametrization $\mathbf{X}(\Theta, X) = \tilde{R}(X)\mathbf{e}_R + X\mathbf{e}_X$, with parameters $0 \le \Theta < 2\pi$, $0 \le X \le L$. We assume $\tilde{R}$ to be smooth, consequently, the outer unit normal vector $\mathbf{n}$, and the surface element dS can be expressed as

$$\mathbf{n} = \frac{\mathbf{e}_R - \tilde{R}'(X)\mathbf{e}_X}{\sqrt{1+\tilde{R}'(X)^2}}, \tag{2a}$$

$$\mathrm{dS} = \tilde{R}(X)\sqrt{1+\tilde{R}'(X)^2}\mathrm{d}\Theta\mathrm{dX}. \tag{2b}$$

As boundary conditions we consider no-slip at the wall of the pipe, and a prescribed constant flow rate $\tilde{Q}$, i.e.,

$$U(X, \tilde{R}(X)) = V(X, \tilde{R}(X)) = 0, \quad 0 \le X \le L \tag{3a}$$

$$\tilde{Q} = \int_{\Gamma_{\text{in}}} U\mathrm{d}S = 2\pi \int_0^{\tilde{R}(0)} RU(X,R)\mathrm{d}R. \tag{3b}$$

2.1 The Darcy Friction Factor

A quantity of interest in the analysis of pipe flow is the pressure drop. The pressure drop is directly related to the mean flow rate, and it determines the power requirements of the device to maintain the flow. In practice, for straight pipes, it is convenient to express the pressure loss as follows [10]

$$\Delta P = f\frac{L}{D}\frac{\rho\bar{U}_0^2}{2}, \tag{4}$$

where, $\Delta P = P_{\text{in}} - P_{\text{out}}$ is the pressure drop over a segment of length L, f is the Darcy friction factor, D is the diameter of the

pipe, ρ is the density and $\bar{U_0}$ is the average of the velocity over the cross section. In the case of laminar flow, i.e., for Poiseuille flow, the friction factor takes the form

$$f = \frac{64}{\mathrm{Re}}, \tag{5}$$

where Re is the Reynolds number, defined as

$$\mathrm{Re} := \frac{\bar{U_0} D}{\nu}. \tag{6}$$

When the radius of the pipe is not constant, one needs to choose a characteristic radius and average velocity, in this paper we select the respective values at the inlet of the pipe, i.e., $D = 2\tilde{R}(0)$ and,

$$\bar{U_0} = \frac{1}{\pi \tilde{R}^2(0)} \int_{\Gamma_{\mathrm{in}}} U \mathrm{dS}. \tag{7}$$

The expression in (4) can be used as a lumped model for describing the flow in any kind of pipe. The main difficulty is to efficiently determine a friction factor that accurately predicts the pressure drop.

2.2 Integral Expression for the Friction Factor

By integrating the axial momentum equation (1a) we can obtain an expression for the pressure loss in terms of surface integrals over the pipe wall Γ. To this purpose, we first rewrite (1a), in the following form

$$\nabla \cdot (U\mathbf{V}) = -\frac{1}{\rho} \nabla \cdot (P\mathbf{e}_X) + \nu \nabla \cdot (\nabla U), \tag{8}$$

where $\mathbf{V} = U\mathbf{e}_X + V\mathbf{e}_R$, and where we used $P_X = \nabla \cdot (P\mathbf{e}_X)$, and $\mathbf{V} \cdot \nabla U = \nabla \cdot (U\mathbf{V})$. Integrating over the domain Ω, see Figure 1, and applying the divergence theorem we get

$$\oint_{\partial\Omega} U\mathbf{V} \cdot \mathbf{n} \mathrm{dS} = -\frac{1}{\rho} \oint_{\partial\Omega} P n_X \mathrm{dS} + \nu \oint_{\partial\Omega} \frac{\partial U}{\partial \mathbf{n}} \mathrm{dS}, \tag{9}$$

where $n_X = \mathbf{n} \cdot \mathbf{e}_X$. Next, we split the surface of integration $\partial\Omega = \Gamma_{\mathrm{in}} \cup \Gamma_{\mathrm{out}} \cup \Gamma$, as sketched in Figure 1. After using the no-slip condition (3a), and rearranging terms we get

$$\begin{aligned} \int_{\Gamma_{\mathrm{in}}} P \mathrm{dS} - \int_{\Gamma_{\mathrm{out}}} P \mathrm{dS} = & \rho \left[\int_{\Gamma_{\mathrm{out}}} U^2 \mathrm{dS} - \int_{\Gamma_{\mathrm{in}}} U^2 \mathrm{dS} \right] + \\ & + \int_{\Gamma} P n_X \mathrm{dS} - \mu \oint_{\partial\Omega} \frac{\partial U}{\partial \mathbf{n}} \mathrm{dS}. \end{aligned} \tag{10}$$

In the following, we restrict ourselves to the case of periodic pipes, i.e., $\tilde{R}(X) = \tilde{R}(X + L)$. In this particular case the expression for the pressure loss derived above simplifies greatly. Since the flow is steady, we can conclude that the velocity field $\mathbf{V}$ is periodic as well, from which it follows that the integrals over Γ_{in}, cancel with the ones over Γ_{out}. In the end, we are left with the following expression for the pressure drop over one period, i.e., from section $X = 0$ to $X = L$,

$$\Delta P = \underbrace{\frac{1}{|\Gamma_{\mathrm{in}}|} \int_{\Gamma} P n_X \mathrm{dS}}_{\Delta P_P} \quad \underbrace{- \frac{\mu}{|\Gamma_{\mathrm{in}}|} \int_{\Gamma} \frac{\partial U}{\partial \mathbf{n}} \mathrm{dS}}_{\Delta P_S}, \tag{11}$$

where n_X is the X-component of the normal vector to the surface, and Γ is the wall of the pipe between $X = 0$ and $X = L$. This formula also tells us that the pressure drop consists of two parts, one due to skin friction, ΔP_S , and one due to the pressure forces acting on the wall of the pipe, ΔP_P. In the particular case of a straight pipe, i.e., for Poiseuille flow, $n_X = 0$ and consequently (11) only contains the integral due to skin friction ΔP_S. After substituting the parabolic profile for U, we recover the result (5), for the laminar friction factor in a straight pipe.

In order to be able to use (11) for computing the friction factor, we need to approximate the normal derivative $\partial U / \partial \mathbf{n}$, and the pressure P at the wall of the pipe. We do this via the method of slow variations.

3 METHOD OF SLOW VARIATIONS

The method of slow variations exploits the geometric characteristics of boundaries that vary more slowly in some direction than others. The key of the method is to rescale the geometry in such a way that the variations become of the same order. This crucial step, enables us to take a geometrical parameter and transfer it as a coefficient in to the scaled equations, which allows us to write the solution as an asymptotic expansion. One of the remarkable properties of the method is that it can handle arbitrarily large variations, provided that they take place slowly [11].

Asymptotic solutions for flow in axially symmetric pipes have been derived in several papers [11–13]. The derivation we present here follows the line of the paper by Kotorynski [13]. Before starting with the method of slow variations, we need to rewrite the Navier-Stokes equations (1) in dimensionless form, by defining the following variables

$$u^* = \frac{U}{\bar{U_0}},\ v^* = \frac{V}{\bar{U_0}},\ x^* = \frac{X}{D},\ r^* = \frac{R}{D},\ p^* = \frac{P}{\rho \bar{U_0}^2}. \tag{12}$$

Substituting these variables in (1) and applying the chain rule we

obtain

$$\mathrm{Re}\,(u^*u^*_{x^*}+v^*u^*_{r^*}) = u^*_{x^*x^*}+u^*_{r^*r^*}+\frac{1}{r^*}u^*_{r^*}-\mathrm{Re}\,p^*_{x^*}, \tag{13a}$$

$$\mathrm{Re}\,(u^*v^*_{x^*}+v^*v^*_{r^*}) = v^*_{x^*x^*}+v^*_{r^*r^*}+\frac{1}{r^*}v^*_{r^*}-\frac{1}{r^{*2}}v^*-\mathrm{Re}\,p^*_{r^*}, \tag{13b}$$

$$u^*_{x^*}+v^*_{r^*}+\frac{1}{r^*}v^* = 0. \tag{13c}$$

3.1 Reformulation in slowly varying variables

Now we proceed to rescale (13), by using the assumption that the radius of the pipe varies slowly in the axial direction. This means that the radius of the pipe $\tilde{R}(X)$ can be written as

$$Dh\left(\frac{\varepsilon}{D}X\right) = \tilde{R}(X), \tag{14}$$

where h is the scaled radius of the pipe, and ε is a small dimensionless parameter characterizing the slow variation of the radius in the axial direction. Such parameter can be taken directly from the expression for the radius if available, for instance if the pipe radius would be of the form $\tilde{R}(X) = (1+\varepsilon^2X^2)^{1/2}$. In the case of a periodic pipe one can consider the maximum variation of the radius a, and compare it to the period of the pipe L, i.e., we define $\varepsilon := a/L$. Then, by applying a proper scaling, we can obtain a domain in which the period is comparable to the variation of the radius. Formally this is done by defining the new variables

$$x = \varepsilon x^*,\ r = r^*,\ u = u^*,\ \varepsilon v = v^*,\ \varepsilon^{-1}p = p^*. \tag{15}$$

Substituting these variables in (13) and multiplying the second and third equations by ε and ε^{-1}, respectively, we obtain

$$\varepsilon\mathrm{Re}\,(uu_x+vu_r) = \varepsilon^2u_{xx}+u_{rr}+\frac{1}{r}u_r-\mathrm{Re}\,p_x, \tag{16a}$$

$$\varepsilon^3\mathrm{Re}\,(uv_x+vv_r) = \varepsilon^4v_{xx}+\varepsilon^2\left(v_{rr}+\frac{1}{r}v_r-\frac{1}{r^2}v_r\right)-\mathrm{Re}\,p_r, \tag{16b}$$

$$u_x+v_r+\frac{v}{r} = 0. \tag{16c}$$

This transfers the parameter ε from the geometry into the equation, where it appears as a coefficient, which allows us to vary this parameter, while keeping the domain fixed, namely $0\le x\le a/D$, and, $0\le r\le h(x)$. Formally this means that we can write an asymptotic expansion for the functions in (16), as follows

$$g(x,r;\varepsilon) = \sum_{i=0}^{\infty} g_i(x,r)\varepsilon^i, \tag{17}$$

where g is a generic variable, $g = u,v,p$. By substituting these expressions into (16), and grouping the variables with respect to their order in ε, we can get a set of equations for each of the orders in the asymptotic expansion. The boundary conditions for the resulting systems are

$$u_i(x,h(x)) = v_i(x,h(x)) = 0, \quad 0\le x\le\frac{a}{D}. \tag{18}$$

In an analogous way, we expand the dimensionless flux Q as $Q = Q_0+\varepsilon Q_1+\varepsilon^2Q_2+\ldots$, where the scaled fluxes Q_i are defined as

$$Q_i := 2\pi\int_0^{h(x)} ru_i(x,r)\mathrm{d}r. \tag{19}$$

Due to continuity, each Q_i is constant, and since the equation must hold for arbitrary ε, it follows that

$$Q_0 = Q, \quad Q_i = 0 \text{ for } i = 2,3,\ldots. \tag{20}$$

Furthermore, the scaled flux can be written as

$$Q_0 = Q = 2\pi\int_0^{h(0)} ru_0(x,r)\mathrm{d}r = \frac{2\pi}{\bar{U_0}}\int_0^{h(0)} rU(0,Dr)\mathrm{d}r, \tag{21}$$

and substituting $\bar{U_0}$ from (7), we get

$$Q_0 = \frac{\pi\tilde{R}^2(0)}{\int_0^{\tilde{R}(0)} RU(0,R)\mathrm{d}R}\int_0^{Dh(0)}\frac{\eta}{D^2}U(0,\eta)\mathrm{d}\eta = \frac{\pi}{4}. \tag{22}$$

3.2 Solving for the leading term

The equations for the leading term can be obtained from (16), by setting $\varepsilon = 0$. The equations read

$$u_{0rr}+\frac{1}{r}u_{0r}-\mathrm{Re}\,p_{0x} = 0, \tag{23a}$$

$$\mathrm{Re}\,p_{0r} = 0, \tag{23b}$$

$$u_{0x}+v_{0r}+\frac{v_0}{r} = 0. \tag{23c}$$

From (23b), we conclude that p_0 is only function of x, and after multiplying (23a) by r and integrating with respect to r we get

$$ru_{0r} = \mathrm{Re}p_{0x}\frac{r^2}{2}+c_1(x). \tag{24}$$

By evaluating the previous expression at $r = 0$ we find $c_1(x) \equiv 0$, and integrating once more with respect to r we get

$$u_0 = \mathrm{Re} p_{0x} \frac{r^2}{4} + c_2(x). \tag{25}$$

Finally, using the no-slip condition at the wall of the pipe, we can determine the function $c_2(x)$, and we obtain

$$u_0 = \frac{\mathrm{Re} p_{0x}}{4} \left(r^2 - h^2(x) \right). \tag{26}$$

Combining (22), and (26) we obtain the following expression for the pressure gradient p_{0x}

$$p_{0x} = -\frac{2}{\mathrm{Re}} \frac{1}{h(x)^4}. \tag{27}$$

Consequently, u_0 takes the form

$$u_0(x,r) = \frac{1}{2h(x)^4} \left(h(x)^2 - r^2 \right). \tag{28}$$

Finally, from (23c), we can determine the radial velocity component v_0. First from (28) we derive

$$u_{0x} = \frac{\left(2r^2 - h(x)^2 \right) h'(x)}{h(x)^5}. \tag{29}$$

Substituting this expression in (23c), integrating w.r.t. r and using the no-slip condition we get

$$v_0 = \frac{r \left(h(x)^2 - r^2 \right) h'(x)}{2h(x)^5} = \frac{r h'(x)}{h(x)} u_0(r,x). \tag{30}$$

Summarizing, the 0th order terms of the asymptotic expansion are

$$u_0(x,r) = \frac{1}{2h(x)^4} \left(h(x)^2 - r^2 \right), \tag{31a}$$

$$v_0(x,r) = \frac{r h'(x)}{h(x)} u_0(r,x), \tag{31b}$$

$$p_0(x,r) = -\frac{2}{\mathrm{Re}} \int_0^x \frac{1}{h(\xi)^4} \mathrm{d}\xi. \tag{31c}$$

This particular expression for p_0 considers setting a reference pressure $p_0(0,0) = 0$. These expressions can be rewritten in terms of the original variables U,V and P, as follows

$$U(X,R) = 2\bar{U}_0 \frac{\tilde{R}(0)^2}{\tilde{R}(X)^2} \left(1 - \frac{R^2}{\tilde{R}(X)^2} \right), \tag{32a}$$

$$V(X,R) = \frac{\tilde{R}'(X)}{\tilde{R}(X)} R U(R,X), \tag{32b}$$

$$P(X,R) = -\frac{16 \rho \bar{U}_0^2 \tilde{R}(0)^3}{\mathrm{Re}} \int_0^X \frac{1}{\tilde{R}(\xi)^4} \mathrm{d}\xi. \tag{32c}$$

4 ESTIMATION OF THE FRICTION FACTOR

In this section we consider two different ways of using the asymptotic solution derived above, in order to find the pressure drop. Naturally the first idea that comes in mind is to directly use expression (32c) and evaluate it at $X = 0$ and $X = L$, thus finding the correspondent pressure drop. The other possibility we consider, is to use the leading terms of the asymptotic expansion (32) for computing the integrals in (11). The first option leads to a result which was originally obtained by Deiber et al. [14], but that unfortunately is not able to capture the dependency on the period L, for the particular case of sinusoidal pipes. The second option is able to capture the dependency on the period L, thus extending the region of applicability of the method. Now we proceed to obtain the two approximations.

Following the first idea, using that p_0 is constant over cross sections, and evaluating (32c), the total pressure loss becomes

$$\Delta P = \frac{16 \rho \bar{U}_0^2 \tilde{R}(0)^3}{\mathrm{Re}} \int_0^L \frac{1}{\tilde{R}^4(X)} \mathrm{d}X. \tag{33}$$

The Darcy friction factor can be obtained by solving for f in (4), this yields

$$f = \frac{64}{\mathrm{Re}} \underbrace{\frac{\tilde{R}(0)^4}{L} \int_0^L \frac{1}{\tilde{R}(X)^4} \mathrm{d}X}_{\mathrm{CF1}}, \tag{34}$$

where CF1 can be interpreted as a correction factor, which when multiplied with the friction factor for laminar flow in straight pipes $64/\mathrm{Re}$, gives us an approximation to the friction factor of an arbitrarily shaped axially symmetric periodic pipe, described by the function $\tilde{R}(X)$. As mentioned before, (34) corresponds to the result previously obtained by Deiber et al. [14]. One of the main advantages of such an estimation, is that it only requires the calculation of a one dimensional integral, consequently obtaining a huge reduction in computation time, when compared to general CFD type methods.

In order to analyze how the approximation with $CF1$ performs, we compare the results obtained with (34) to those ob-

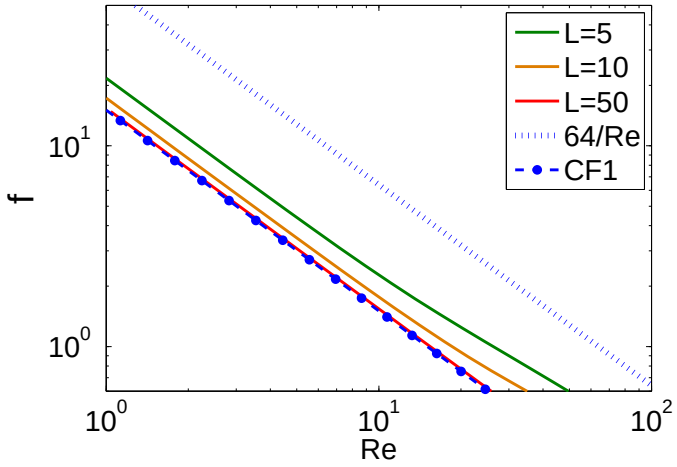

FIGURE 2. Friction factor (solid lines) and approximation obtained with correction factor $CF1$ (34)(dotted lines), as function of the Reynolds number, for a sinusoidal pipe depicted as in Figure 5. Parameter values are $D = 2$, and $a = 1$. The estimation obtained with $CF1$ is the same for all the values of L.

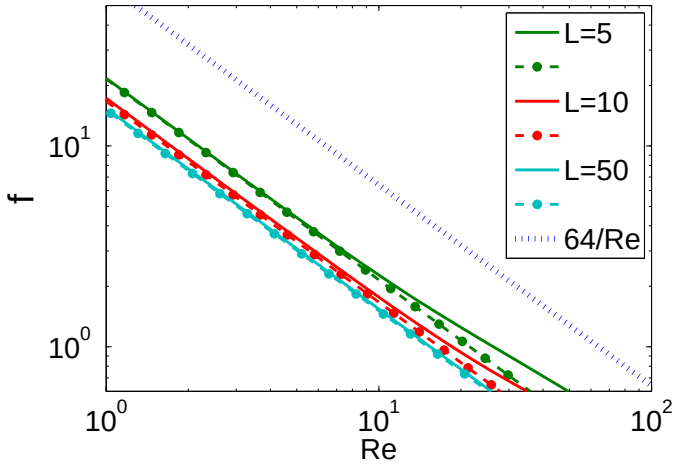

FIGURE 3. Friction factor (solid lines) and approximations obtained with correction factor $CF2$ (41) (dotted lines), as function of the Reynolds number, for a sinusoidal pipe depicted as in Figure 5. Parameter values are $D = 2$, and $a = 1$.The estimation with $CF2$ is able to capture the changes in friction factor due to changes in the period L.

tained with the CFD methodology, that will be described in Section 5. For the simulations we consider a sinusoidal pipe depicted as in Figure 5. In Figure 2 we show the variation of the friction factor with Reynolds number for a sinusoidal pipe with amplitude $a = 2$, and different values of L. We notice the deviation of the friction factor computed with CFD (solid lines), from the friction factor for straight pipes $64/\mathrm{Re}$ (dotted line). The friction factor obtained with (34), unfortunately, is not able to capture the dependency on the parameter L, for this set of examples, and it gives the same result regardless of L. Nonetheless, we can observe how the results obtained with CFD approach the estimation obtained with the correction factor $CF1$, as the period of the pipe L, increases. In order to be able to capture the dependency on the parameter L, we proceed to the second alternative.

Instead of using the asymptotic solution directly, we substitute the asymptotic solution (32) into the integral expression for the pressure drop (11), and perform the correspondent integrations. First we derive the pressure loss due to pressure forces on the wall ΔP_P. Using the expressions for the normal vector (2a) and the surface element (2b), we obtain

$$\begin{aligned}\Delta P_P &:= \frac{1}{|\Gamma_{\text{in}}|}\int_\Gamma P n_X \,\mathrm{d}S \\ &= \frac{32\rho\bar{U}_0^2\tilde{R}(0)}{\mathrm{Re}}\int_0^L\left(\int_0^X \frac{1}{\tilde{R}(\xi)^4}\mathrm{d}\xi\right)\tilde{R}(X)\tilde{R}'(X)\mathrm{d}X.\end{aligned} \tag{35}$$

Changing the order of integration we get

$$\Delta P_P = \frac{16\rho\bar{U}_0^2\tilde{R}(0)}{\mathrm{Re}}\left[\tilde{R}(L)^2\int_0^L\frac{1}{\tilde{R}(X)^4}\mathrm{d}X - \int_0^L\frac{1}{\tilde{R}(X)^2}\mathrm{d}X\right]. \tag{36}$$

In the same way, using (32) and (2a), we can obtain the pressure loss due to skin friction. First we compute

$$\begin{aligned}\frac{\partial U}{\partial R} &= -4\bar{U}_0\tilde{R}(0)^2\frac{R}{\tilde{R}(X)^4}, \\ \frac{\partial U}{\partial X} &= 4\bar{U}_0\tilde{R}(0)^2\frac{\tilde{R}'(X)}{\tilde{R}(X)^3}\left[2\frac{R^2}{\tilde{R}(X)^2}-1\right].\end{aligned} \tag{37}$$

Then we can evaluate $\nabla U\cdot\mathbf{n}$ at the wall Γ and get

$$\begin{aligned}\Delta P_S :=& -\frac{\mu}{|\Gamma_{\text{in}}|}\int_\Gamma\frac{\partial U}{\partial\mathbf{n}}\mathrm{d}S \\ =& 8\mu\bar{U}_0\int_0^L\frac{1}{\tilde{R}(X)^2}\left[1+\left(\tilde{R}'(X)\right)^2\right]\mathrm{d}X.\end{aligned} \tag{38}$$

Adding the pressure loss due to forces on the wall (36) with the pressure loss due to skin friction (38), we get the following approximation for the total pressure loss

$$\begin{aligned}\Delta P =& \frac{16\rho\bar{U}_0^2\tilde{R}(0)}{\mathrm{Re}}\left[\tilde{R}(L)^2\int_0^L\frac{1}{\tilde{R}(X)^4}\mathrm{d}X - \int_0^L\frac{1}{\tilde{R}(X)^2}\mathrm{d}X\right]+ \\ &+8\mu\bar{U}_0\int_0^L\frac{1}{\tilde{R}(X)^2}\left[1+\left(\tilde{R}'(X)\right)^2\right]\mathrm{d}X.\end{aligned} \tag{39}$$

Grouping terms and using $\rho D\bar{U}_0/\mu \mathrm{Re} = 1$, we finally get

$$\Delta P = \frac{16\rho \bar{U}_0^2 \tilde{R}(0)}{\mathrm{Re}} \int_0^L \frac{\tilde{R}'(X)^2}{\tilde{R}(X)^2} + \frac{\tilde{R}(0)^2}{\tilde{R}(X)^4} \mathrm{d}X, \tag{40}$$

which in terms of a friction factor yields

$$f = \frac{64}{\mathrm{Re}} \underbrace{\frac{\tilde{R}(0)^2}{L} \int_0^L \frac{\tilde{R}'(X)^2}{\tilde{R}(X)^2} + \frac{\tilde{R}(0)^2}{\tilde{R}(X)^4} \mathrm{d}X}_{\mathrm{CF2}}. \tag{41}$$

This gives us an alternative expression for approximating the friction factor, that in contrast with (34), is able to capture the dependency on the parameter L, as it can be observed in Figure 3. The estimations obtained with our new approximation (41) are displayed in dotted lines, and the results obtained with CFD in solid lines, the line corresponding to $64/\mathrm{Re}$ is displayed for reference. The estimate (34) accurately predicts the friction factor up to certain Reynolds number, at which inertial effects become more important.

Since it is always instructive to compare results with experimental data. In Figure 4 we show a plot of experimental data (blue dots), and two-dimensional numerical simulation (green solid line), obtained by Deiber et al. [14, p. 642]. The estimation obtained with (41) is displayed in a red dashed line. The two-dimensional numerical simulation by Deiber et al., was obtained by means of an iterative technique in which the shape is slowly altered from a reference configuration. Their experiments, were conducted in a sinusoidal pipe, which in terms of our parameters; see Figure 5, correspond to $a = 0.8571$ and $L = 8.9714$. The estimation obtained with (41) matches both plots up to a Reynolds number of approximately $\mathrm{Re} \approx 162$. For larger Reynolds number, the estimation starts to deviate from the experimental data, while the two-dimensional numerical solution follows to some extend, till at $\mathrm{Re} \approx 750$, a change towards turbulence can be observed from the experimental data, and nor the estimate, nor the numerical solution, are expected to correctly describe the flow.

One of the most important advantages of (41) is that it is able to follow the effects due to changes in the period L, while the computational cost are still those of numerical integration in one dimension. For instance a typical computation time for (41), with an adaptive quadrature rule, with a tolerance of $\mathrm{tol} = 10^{-6}$ in MatLab, ranges from 6.01×10^{-3}, to 7.83×10^{-3} seconds. In contrast the computation times of the CFD implementation (Comsol) presented in Section 5, range from 20, to 51 seconds, for a fine mesh (1039 mesh points), and from 11, to 36 seconds, for a coarse mesh (212 mesh points), achieving a huge reduction in computation time. The parameters of the geometry for this computations were varied from $a = 0$ to $a = 2$, $L = 0$ to $L = 80$, and $\mathrm{Re} \approx 10$ to $\mathrm{Re} \approx 1200$. The coarse mesh was considered mostly for time comparison purposes, in this case the

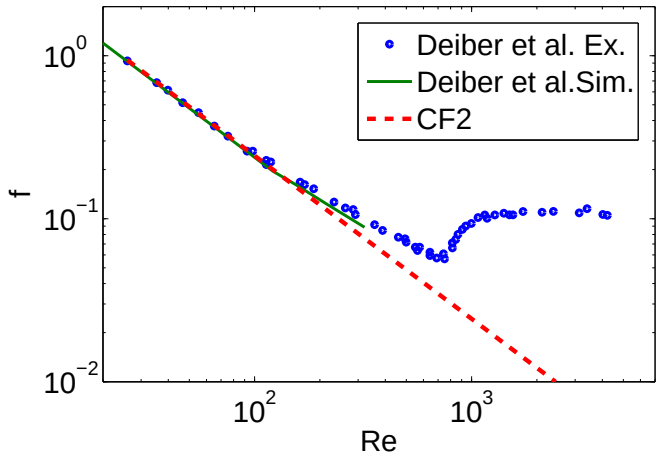

FIGURE 4. Experimental results (blue dots), 2D numerical solution (solid green line) for the friction factor by Deiber et al. [14, p. 642], and approximation obtained with correction factor $CF2$ (41) (dashed line), as function of the Reynolds number, for a sinusoidal pipe depicted as in Figure 5. Parameter values are $D = 2$, $a = 0.8571$ and $L = 8.9714$; all the values were converted from the variables used in Deiber et al. [14], to the ones used in this paper.

CFD solver did not converge for all the geometries, specially in the case $a/L \gg 1$. The simulations with the fine mesh, converged in all cases.

The natural question at this point is to know more precisely, how accurate this estimation works, and in which cases the method is applicable.

5 VALIDATION OF THE METHOD

Above it was shown that (41) provides better approximations than (34). In order to analyze the accuracy of our method for estimating the friction factor, we compare the results obtained using (41), with the results obtained with CFD computations. To this extend we consider pipes with sinusoidal walls depicted as in Figure 5, where a and L, are the amplitude and period of the sinusoidal function, respectively. The geometry is chosen in such a way that the radius is 1 at the inlet. The radius can be written as

$$\tilde{R}(X) = 1 + \frac{a}{2}\left(1 + \sin\left(\frac{2\pi}{L}X - \frac{\pi}{2}\right)\right), \tag{42}$$

which translates into

$$h(x) = \frac{1}{2} + \frac{a}{4}\left(1 + \sin\left(\frac{\pi x}{a} - \frac{\pi}{2}\right)\right). \tag{43}$$

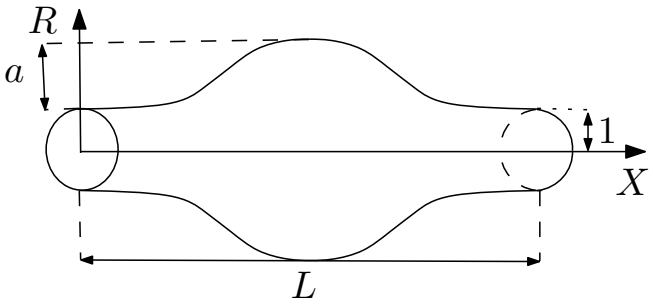

FIGURE 5. Sinusoidal pipe with center line along the X-axis, a and L stand for the amplitude and period of the sine function, respectively.

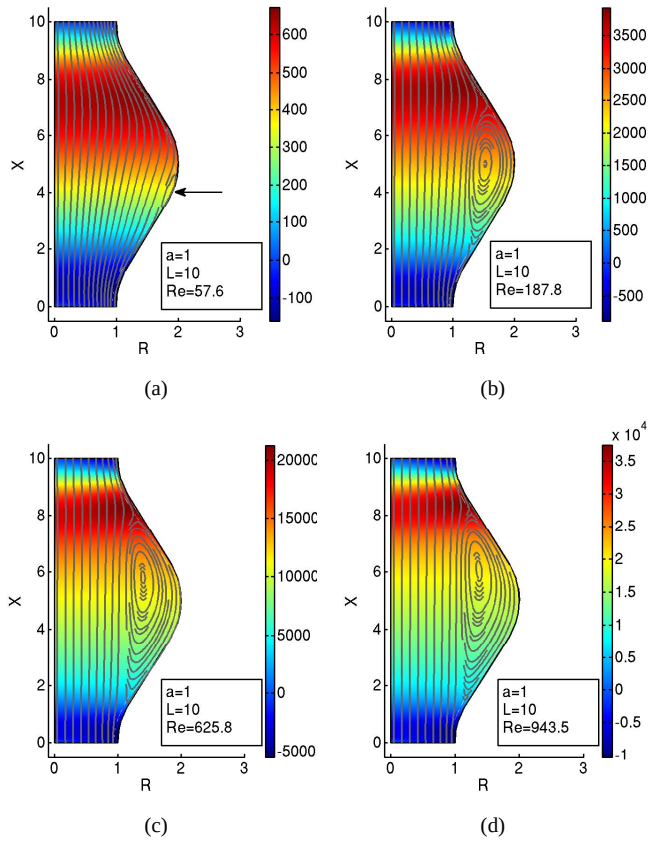

FIGURE 6. Pressure fluctuations $\tilde{P}$, and velocity streamlines for a sinusoidal pipe with radius at inlet $\tilde{R}(0) = 1$, amplitude $a = 1$, period $L = 10$, and different Reynolds numbers.

5.1 CFD Methodology

The computation domain can be reduced to just one period, when the flow is fully developed, due to the following argument. Since the geometry under consideration is periodic, it is plausible to assume that all velocity components are periodic as well. The pressure can be split as follows

$$P(X,R) = \tilde{P}(X,R) + fX, \tag{44}$$

where $\tilde{P}(X,R)$ represents the fluctuations due to the presence of the corrugation, and f is the Darcy friction factor. This transformation is also used in the papers by van der Linden, et.al. [9], and Pisarenco, et.al. [8].

The main advantage of this reformulation is that $\tilde{P}$ is also periodic, thus allowing to reduce the domain to just one period. The implementation works as follows, first we prescribe a pressure gradient (friction factor) f, which is included as a force term in the Navier-Stokes equations, with variables U, V and $\tilde{P}$, i.e. we solve for the pressure fluctuation $\tilde{P}$, instead of the original pressure P. Second we solve the periodic Navier-Stokes equations, and compute the average velocity $\bar{U}_0$, by integrating the axial velocity component U over the inlet of the pipe. Finally, we determine the resulting Reynolds number according to $\mathrm{Re} = \bar{U}_0 a/\nu$. The Navier-Stokes equations are solved with a finite element code (Comsol Multiphysics [15]), using Lagrange P2-P1 elements, and a boundary layer mesh, the discretized equations were solved using a direct sparse solver (UMFPACK) [15], with a tolerance of tol $= 10^{-6}$.

In Figure 6 we show the fluctuation of the pressure $\tilde{P}$, and the velocity streamlines obtained for a sinusoidal pipe with amplitude $a = 1$ and period $L = 10$. Due to axial symmetry, it is enough to solve just one of the symmetric sides of the pipe. The center line is located at $R = 0$, the wall of the pipe appears on the right side of the picture, and the flow direction is upwards. For the small Reynolds number $\mathrm{Re} = 57.6$, one can observe, signaled by an arrow, the onset of a small vortex close to the deepest part of the protrusion. In this case, our approximation to the friction factor delivers a relative error of 10%. For $\mathrm{Re} = 187.8$ we can observe a vortex completely filling the protrusion of the pipe, but the center of the vortex coincides with the center of the corrugation and our approximation delivers a relative error of about 20%. For higher Reynolds numbers, $\mathrm{Re} = 625.8, 943.5$, the center of the vortex shifts towards the upper part, and then formula (41) losses precision, yielding 30% relative error for the case in Figure 6(c), and 40% relative error for the case in Figure 6(d). For the pressure fluctuations, we can observe that, for moderate Reynolds numbers, the pressure is constant over the cross sections, and it starts to vary over the cross section $X = 8.5$ at $\mathrm{Re} = 943.5$; see Figure 6(d). The method provides good approximations provided that the flow stays laminar, and the size of the vortices are small, or are centered around the middle point in the axial direction, in this particular case at $X = 5$.

5.2 Applicability of the method

In order to investigate the accuracy and range of applicability of our approximation to the friction factor (41) systematically,

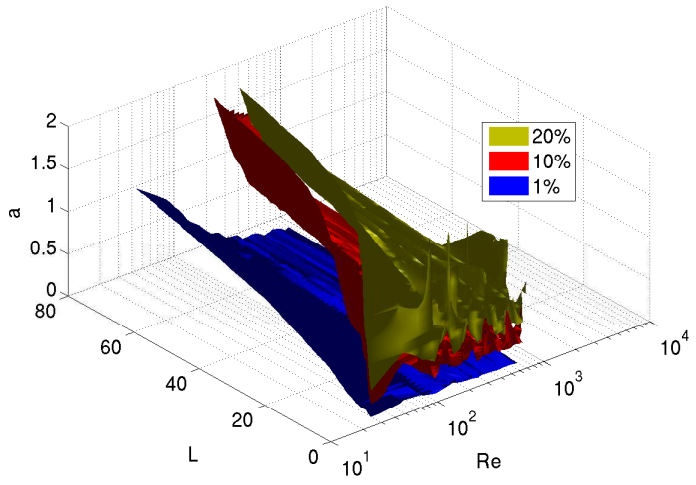

FIGURE 7. Isosurfaces for the relative error at values $Err = 1\%$, $Err = 10\%$, and $Err = 20\%$. The surfaces appear in the parameter space determined by Re, L, and a.

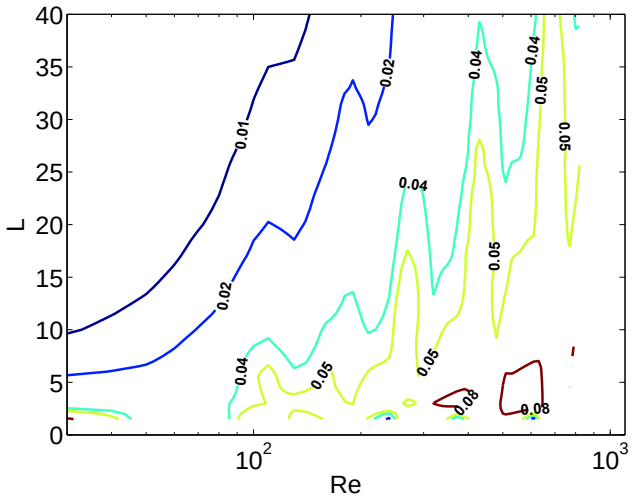

FIGURE 8. Contours of the relative error Err, for a sinusoidal pipe with amplitude $a = 0.2$ as function of the Reynolds number Re, and the period of the pipe L.

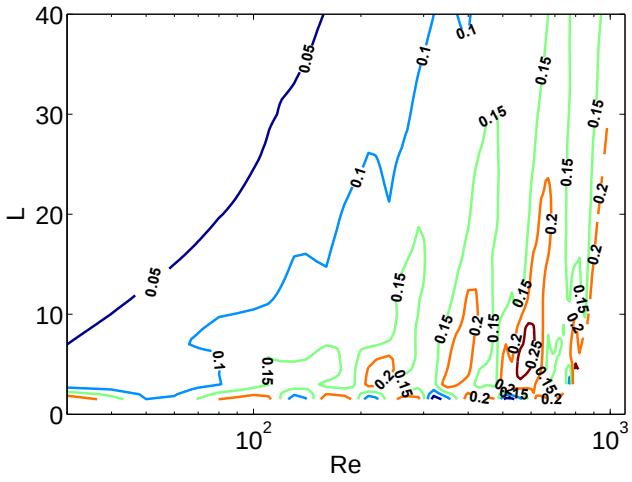

FIGURE 9. Contours of the relative error Err, for a sinusoidal pipe with amplitude $a = 0.5143$ as function of the Reynolds number Re, and the period of the pipe L.

we considered the case of sinusoidal pipes, and varied the geometry parameters, ranging from 0 to 2 for the amplitude of the pipe a, from 0 to 80 for the period of the pipe L, where the geometry had been previously rescaled for having a reference radius at the inlet of $\tilde{R}(0) = 1$. Then we compared these estimations to the results obtained using the CFD approach, as described above, and computed the respective relative error Err as

$$Err := \frac{|f - \tilde{f}|}{|f|}, \tag{45}$$

with f being the friction factor obtained from the steady numerical solver, and $\tilde{f}$ our estimation to the friction factor calculated from (41).

The results from these tests are shown in Figure 7. The regions in the parameter space, were the method delivers approximations with relative errors $Err = 1\%$, $Err = 10\%$, and $Err = 20\%$ are presented as isosurfaces. The zones below each of the isosurfaces, constitute a region where our approximation yields a relative error smaller than the corresponding error of the isosurface. For instance, if the period of the pipe is $L = 80$, and the Reynolds number $\mathrm{Re} = 50$, our approximation yield and error smaller than $Err = 1\%$, for any amplitude $0 \leq a \leq 1$.

In order to give a more clear impression of the regions of accuracy of the method, we show cross sections of the error for some fixed values of the amplitude a, as function of Re and L. The results are displayed in terms of contour lines of the error. Figure 8 shows the results for the case $a = 0.2$. Some remarkable property, is the fact that the maximum error in the whole region is only 8%. Of course this accuracy can not be attained for all parameter values. When one increases the size of the amplitude, the accuracy of the method decreases, for instance when $a = 0.5143$, Figure 9, there are still some regions where the accuracy is of the order of 5%, but in other regions the error increases up to 25%. For the case $a = 1$, Figure 10, the region of 5% accuracy is reduced, and some zones with error of up to 30% appear.

We note that for large values of Re, and a/L, (i.e. in the lower right corners in Figs. 10,8, and 9), the flow could already be in the turbulent region. In such kind of situation, the computed

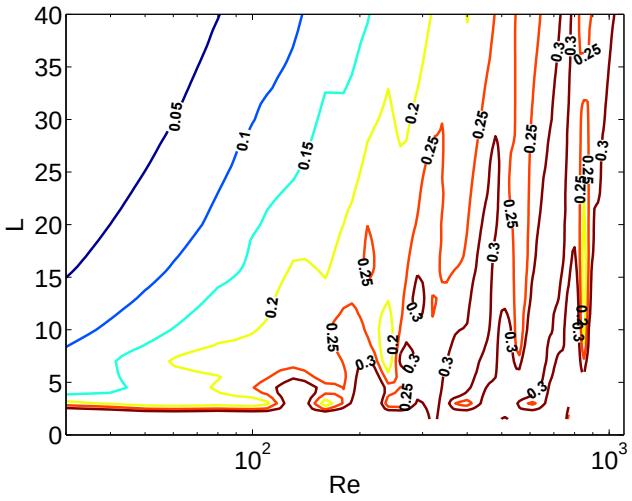

FIGURE 10. Contours of the relative error Err, for a sinusoidal pipe with amplitude $a = 1$ as function of the Reynolds number Re, and the period of the pipe L.

steady solution is not valid, and consequently the plotted errors are unlikely to be accurate.

6 CONCLUSIONS

Based on asymptotic solutions obtained from the method of slow variations, and on an integral expression for the friction factor, in this paper we derived approximate expressions for the friction factor in axially symmetric pipes. Estimating the friction factor with these expressions, requires only numerical integration in one dimension, and consequently the method is extremely efficient. Reducing from a typical computation type of 11 seconds for CFD type methods, to just 6×10^{-3} seconds.

From the validation with sinusoidal pipes, we can conclude that our method yields an error smaller than 10%, for amplitude values up to $a = 0.2$. For larger amplitudes, we additionally require, roughly speaking, either a small Reynolds number Re, or a large value of L, for keeping the error below 10%. The maximum error in the range of parameters investigated here, is about 25%, and 30%, for amplitudes $a = 0.5143$, and $a = 1$, respectively.

ACKNOWLEDGMENT

This work is part of a project in collaboration with Stork FDO Inoteq and it is funded by Ballast Nedam IPM.

REFERENCES

[1] Witz, J. A., Ridolfi, M. V., and Hall, G. A., 2004. "Offshore LNG transfer - a new flexible cryogenic hose for dynamic service". Offshore Technology Conference.

[2] Moody, L. F., 1944. "Friction factors for pipe flow". *Trans. ASME*, ***66***(8), November, pp. 97–107.

[3] Nikuradse, J., 1933. Stormungsgesetz in rauhren rohren, vDI Forschungshefte 361 (English translation: Laws of flow in rough pipes.). NACA Technical Memorandum 1292, National Advisory Commission for Aeronautics, Washington, DC, USA.

[4] Lessen, M., and Huang, P.-S., 1976. "Poiseuille flow in a pipe with axially symmetric wavy walls". *The Physics of Fluids*, ***19***(7), July, pp. 945–950.

[5] Inaba, T., Ohnishi, H., Miyake, Y., and Murata, S., 1979. "Laminar flow in a corrugated pipe". *Bulletin of the JSME*, ***22***(171), September, pp. 1198–1204.

[6] Blackburn, H. M., Ooi, A., and Chong, M. S., 2007. "The effect of corrugation height on flow in a wavy-walled pipe". In 16th Australasian Fluid Mechanics Conference, A. Editor and B. Editor, eds., pp. 559–564.

[7] Mahmud, S., Sadrul Islam, A. K. M., and Feroz, C. M., 2003. "Flow and heat transfer characteristics inside a wavy tube". *Heat and Mass Transfer*(39), pp. 387–393.

[8] Pisarenco, M., van der Linden, B. J., Tijsseling, A., Ory, E., and Dam, J., 2009. "Friction factor estimation for turbulent flows in corrugated pipes with rough walls". In Proceedings of the ASME 28th International Conference on Ocean, Offshore and Arctic Engineering, ASME. OMAE2009-79854.

[9] Van der Linden, B. J., Ory, E., Dam, J., Tijsseling, A. S., and Pisarenco, M., 2009. "Efficient computation of three-dimensional flow in helically corrugated hoses including swirl". In Proceedings of 2009 ASME Pressure Vessels and Piping Conference. PVP2009-77997.

[10] Cengel, Y. A., and Cimbala, J. M., 2006. *Fluid Mechanics: Fundamentals and Applications*. McGraw Hill.

[11] Van Dyke, M., 1987. "Slow variations in continuum mechanics". In *Advances in applied mechanics*, T. Y. Wu and J. W. Hutchinson, eds., Vol. 25. Academic Press, Inc., San Diego, CA, pp. 1–45.

[12] Manton, M. J., 1971. "Low reynolds number flow in slowly varying axisymmetric tubes". *J. Fluid Mech.*, ***49***(3), Jan, pp. 451–459.

[13] Kotorynski, W. P., 1995. "Viscous flow in axisymmetric pipes with slow variations". *Computers & Fluids*, ***24***(6), pp. 685–717.

[14] Deiber, J. A., and Schowalter, W. R., 1979. "Flow trough tubes with sinusoidal axial variations in diameter". *AIChE Journal*, ***25***(4), pp. 638–645.

[15] COMSOL, 2006. *User's Guide. COMSOL AB.*